CrossMark

ORIGINAL PAPER

Fabrication and characterization of zinc oxide-decorated titania nanoporous by electrochemical anodizing-chemical bath deposition techniques: visible light active photocatalysts with good stability

Mohamad Mohsen Momeni[1] · Yousef Ghayeb[1]

Abstract ZnO-decorated titania nanoporous (ZnO/TNPs) nanocomposites were fabricated by electrochemical anodizing-chemical bath deposition and characterized by SEM, EDX and XRD. Results showed that titania nanoporous with an inner average pore diameter of 80–110 nm and a length of 40 μm are grown on titanium foils. ZnO is decorated on titania nanoporous by a chemical bath deposition technique. Diffuse reflectance spectra showed an increase in the visible absorption relative to bare titania nanoporous. The ZnO was successfully decorated on the titania nanoporous, which enhanced the photocatalytic activity of the ZnO/TNPs, as indicated by the efficient removal of methylene blue. The resultant ZnO decorated titania nanoporous showed better photocatalytic activity than the bare titania under visible light radiation. Such photocatalyst benefits from the capability of high specific surface and the direct conduction path through the aligned nanoporous. This inexpensive photocatalyst prepared free of noble metals, showed enhanced high photocatalytic activity with good stability.

**Keywords** Nanoporous · ZnO · Titania · Visible light · Photocatalysts

Introduction

One-dimensional (1-D) nanostructured semiconducting materials, such as nanorods, nanowires, and nanotubes have garnered considerable attention because of their unique physical and chemical properties [1–4]. Among one-dimensional inorganic nanostructures, titania nanotube to date has been extensively pursued as main photocatalyst by virtue of high surface-to-volume ratio and superior physicochemical properties [4]. Various routes have been developed for fabricating titania nanotube. Nevertheless, these methods often confront problems of template removal, tedious operation procedures and poor adhesion of nanotube to the underlying substrate [5–8]. In contrast, anodic oxidation of titanium leading to vertically aligned titania nanotube arrays, as an alternative strategy, has prompted burgeoning interest, which possesses virtues of simplicity and efficiency, and moreover, it represents a unique combination of highly functional features of titania with a regular and controllable nanoscale geometry [4, 9–11]. Titania nanotube arrays prepared via anodization of titanium foil possess high surface-to-volume ratios and fast charge transport property, which are often considered to be advantageous for applications requiring efficient surface reactivity [12–15]. However, previous studies on the applications of titania nanotube have found that the high recombination rate of photogenerated electron–hole pairs and wide band gap (E_g ~3.2 eV) were the main drawbacks that limited the photocatalytic activity and visible light response of titania nanotube [12, 16, 17]. An efficient approach is loading of titania with some semiconductors to form heterojunctions, such as WO_3, SnO_2, CdS, CeO_2, V_2O_5 and so on which can enhance interfacial electrons transfer to the underlying metal substrate [18–25]. ZnO is an important semiconductor with a band gap of 3.37 eV and exhibits higher electron mobility and longer life time of carriers than TiO_2 [26]. Recently, a few investigations have been carried out for design and preparation of nanocomposites containing ZnO and TiO_2 [27–37]. It has been realized that mixed ZnO–TiO_2 displays profoundly

✉ Mohamad Mohsen Momeni
mm.momeni@cc.iut.ac.ir

[1] Department of Chemistry, Isfahan University of Technology, 84156-83111 Isfahan, Iran
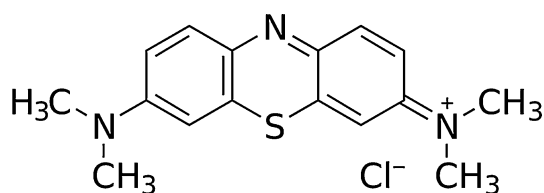
Fig. 1 Structure of methylene blue (MB)

improved properties and high efficiency as compared to the pure ZnO and TiO$_2$ materials.

In this study, we construct ZnO-decorated titania nanoporous (ZnO/TNPs) nanocomposites via efficient and easily accessible approach. The decoration of zinc occurs homogenously and ZnO-decorated titania nanoporous films can be achieved using chemical bath deposition (CBD) technique. This method makes it more favorable for the deposition in the tubes, and provides a general way for any mesoporous or microporous substrate where this type of selective deposition is desired. To the best of our knowledge, report on the preparation of ZnO-decorated titania nanoporous films by anodizing and following chemical bath deposition is lacking. Also, to our knowledge, the quantity effect of zinc in titania nanoporous (ZnO/TNPs) on photocatalytic activities of ZnO/TNPs are lacking. In this paper, two-step process was developed to prepare ZnO/TNPs composite films. In the first step, titania nanoporous were prepared by anodizing titanium foils. Then zinc was deposited on these nanoporous by a chemical bath deposition technique. The morphology and structure were characterized by scanning electron microscopy (SEM), energy-dispersive X-ray spectroscopy (EDX) and X-ray diffraction (XRD). Optical properties were investigated by UV–Visible diffuse reflectance spectra (UV/vis/DRS). The effect of ZnO-decorated titania on the photocatalytic activity of these samples was investigated by degradation of methylene blue. Methylene blue (MB) is a cationic dye, used extensively for dying cotton, wool and silk. The risk of the existence of this dye in waste water may be arisen from the burning effect of eye, nausea, vomiting and diarrhea. MB has a maximum absorption in the 660 nm visible area. Methylene blue is chosen as model contaminant to evaluate the photocatalytic activities of ZnO/TNPs samples due to its stability under visible light irradiation. Chemical structure (drawn by ChemDraw software) of methylene blue (C$_{16}$H$_{18}$N$_3$SCl) makes it to fall under a group of azin dyes as shown in Fig. 1.

Experimental

All chemicals were of analytical grade without further purifying before experiment and solutions were prepared with distilled water.

A piece of titanium sheet (99.99 % purity, 1-mm thick) was cut into desired dimension and the titanium electrode was mechanically polished with different emery-type abrasive papers (with the following grades: 60, 80, 600, 1200 and 2500), rinsed in a bath of distilled water, and then chemically etched by immersing in a mixture of HF and HNO$_3$ acids for 30 s. The ratio of components HF/HNO$_3$/H$_2$O in the mixture was 1:4:5 in volume. The last step of pretreatment was rinsing with distilled water. After cleaning, anodic films were grown from titanium by anodizing titanium foil in a solution of ethylene glycol (98 mL) containing 0.1 M ammonium fluoride and 2 mL distilled water at a constant voltage of 60 V for 6 h at room temperature using a graphite foil with about 12 cm^2 geometric areas as cathode. After anodization of titanium and preparation of titania nanoporous, ZnO was decorated on nanoporous by chemical bath deposition. The titania nanoporous (TNPs) were soaked in a 0.1 M H$_2$SO$_4$ solution for 90 min followed by soaking in a H$_2$O/ethanol (4:1) solution containing 0.05 M ZnSO$_4$·7H$_2$O for different times at 70 °C. The samples were rinsed with distilled water and dried in air. Then, samples were annealed by heating at 400 °C for 2 h in a tube furnace (Azar Furnace), with a ramp of 2 °C/min to form zinc oxide and also to obtain crystalline samples that lead to ZnO/TNPs with varied weight loading percentage of 1, 3 and 5 %. In the present work, we compare the photocatalytic performance of bare titania nanoporous (TNPs) and titania nanoporous decorated with different quantity of zinc oxide referred to as ZnO/TNPs1, ZnO/TNPs2 and ZnO/TNPs3. Table 1 summarizes the experimental conditions for 4 different samples. A schematic of the pretreatment method of titanium sheets and process of producing ZnO decorated on titania nanoporous on titanium foils is shown in Fig. 2.

The surface morphologies of all samples were characterized by field emission scanning electron microscopy (FE-SEM, Hitachi S-4160, Japan), and the elemental composition was estimated by energy-dispersive X-ray spectroscopy (EDX). The crystalline phases were identified by XRD (Philips X'Pert). Diffraction patterns were recorded in the 2θ range from 20° to 80° at room temperature. The optical absorption of the samples was determined using a diffuse reflectance UV–Visible (DRUV-Vis) spectrophotometer (JASCO V-570). The values of the band gap energy (E_g) were calculated using the following equation:

$$(\alpha h\upsilon) = A\left(h\upsilon - E_g\right)^n \tag{1}$$

where E_g is the band gap energy, h is Planck's constant, υ is the frequency of vibration, $h\upsilon$ is the incident photon energy, A is a proportional constant and α is the absorption coefficient per unit length [19]. The band gap values were determined by extrapolating the linear region of the plot to $h\upsilon = 0$.

Table 1 The experimental parameters for the synthesis of different samples

Samples	Anodizing solution	Chemical bath deposition in H_2O/ethanol (4:1) solution containing 0.05 M $ZnSO_4·7H_2O$
TNPs	98 mL EG + 2 mL H_2O + 1 mM NH_4F (60 V, 6 h at room temperature)	–
ZnO/TNPs1	98 mL EG + 2 mL H_2O + 1 mM NH_4F (60 V, 6 h at room temperature)	Soaking for 1 h at 70 °C
ZnO/TNPs2	98 mL EG + 2 mL H_2O + 1 mM NH_4F (60 V, 6 h at room temperature)	Soaking for 3 h at 70 °C
ZnO/TNPs3	98 mL EG + 2 mL H_2O + 1 mM NH_4F (60 V, 6 h at room temperature)	Soaking for 5 h at 70 °C
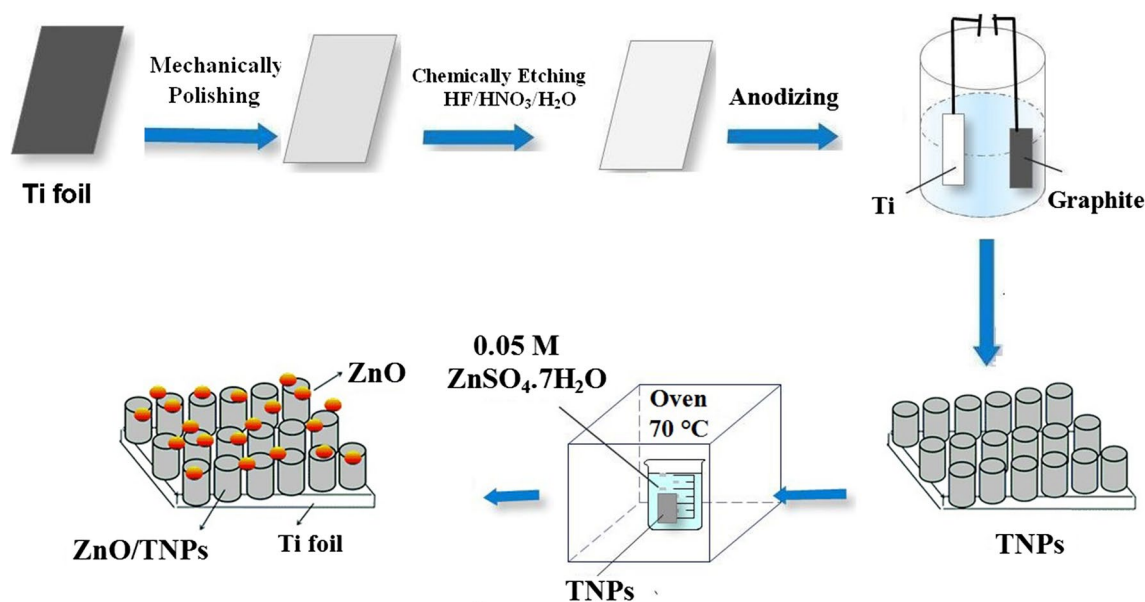
Fig. 2 Schematic presentation of the pretreatment method of titanium sheets and process of producing ZnO-decorated titania nanoporous (ZnO/TNPs) nanocomposites on titanium foils

Photocatalytic activities of all the samples were evaluated by degradation of the aqueous methylene blue (MB) under visible light irradiation. The photocatalytic reaction was carried in a single-compartment cylindrical quartz reactor. A 200 W xenon lamp was used as a light source. The luminous intensity of the xenon lamp was 100 mW/cm². Light was transmitted by the quartz glass as the xenon lamp shone on the samples. A fan was used to cool down the reactor tube. The actual experiments were performed at room temperature. The initial concentration of methylene blue was 2 mg/L. The volume of the solution was 50 mL. Prior to illumination, the photocatalyst sample was immersed in quartz reactor containing methylene blue and magnetically stirred for 2 h in the dark to ensure the establishment of an adsorption–desorption equilibrium between the photocatalyst and methylene blue. Then the solution was exposed to visible light irradiation under magnetic stirring for 2 h. At each 10-min intervals, 5 mL solution was sampled and the absorbance of methylene blue was measured by a UV–Vis spectrophotometer.

Results and discussion

The FE-SEM of the as-prepared samples is illustrated in Fig. 3. Figure 3a–c shows the top view of different ZnO-decorated titania nanoporous (ZnO/TNPs) samples formed by chemical bath deposition. All samples displayed ordered nanoporous with the diameter of the tubes around 80–110 nm, and wall thickness is estimated to be in the range of 30–60 nm. From the cross-sectional view in Fig. 3d, it can be seen that the formed nanoporous are parallel aligned and have a length in the range of ~39 μm.

XRD was employed to characterize the crystal structure of ZnO/TNPs as well as that of bare titania nanoporous (TNPs). Figure 4 illustrates the XRD patterns of the as-fabricated and annealed ZnO/TNPs samples annealed at 400 °C together with that of the bare TNPs for comparison. It confirms the presence of anatase phase of TiO_2 in the samples and the Ti peaks were due to the titanium substrate. XRD pattern of the synthesized ZnO/TNPs shows the diffraction peaks of both ZnO and TiO_2. Peaks appear at 2θ: 25.4, 37.0, 37.9, 54.0, 55.2, 68.9, 70.4, 75.2 and 76.2 corresponding to the diffraction patterns of (101), (103), (004), (105), (211), (116), (220), (215) and (301), respectively, of the pure anatase phase of TiO_2. Crystalline zinc oxide with hexagonal structure showed main peaks at $2\theta = 36.2$, 47.5, 56.5, 62.8, 69 and 76.9, which are in exact agreement with standard card [38].

The successful formation of ZnO on the titania nanoporous was also confirmed through energy-dispersive X-ray spectroscopy (EDX) spectra obtained from different samples (Fig. 5). It was seen that the films mainly consisted of Ti, O and Zn. In addition to the peaks at ~4.5 and ~0.5 keV, which correspond to Ti Ka and Ti La, respectively, peaks at ~0.4 and ~4.9 keV appeared in the EDX spectra of samples. The peaks observed at ~8.6 and ~1.0 keV correspond to Zn Ka and Zn La, respectively. The occurrence of traces

of contaminants such as carbon and sulfur from precursors is also observed. The presence of carbon originated from absorption of carbon from ethylene glycol. It is believed that carbon species adsorb onto the surface during anodization and subsequent heat treatment induces diffusion into the crystal structure of TiO_2 [19].

Regarding the UV–Vis spectra recorded data; the absorption edge of sample ZnO/TNPs3 was closer to the visible light region than that of other samples. The typical plot of $(\alpha h\upsilon)^{1/2}$ vs. photon energy ($h\upsilon$) is depicted in Fig. 6 with the extrapolated linear portion corresponding to the E_g value. The incorporation of zinc oxide extended the ability of TiO_2 to respond to higher wavelengths. Concerning to the band gap energy (E_g) values, there was a visible shift in the absorption edge for sample ZnO/TNPs3 ($E_g = 2.85$ eV) compared to the sample ZnO/TNPs2 ($E_g = 2.95$ eV), sample ZnO/TNPs1 ($E_g = 3.05$ eV) and sample TNPs ($E_g = \sim 3.18$ eV). Compared with bare TNPs, all of the ZnO/TNPs samples exhibit a red shift of absorption edge and band gap decrease with the increase of zinc concentration. To the author's best knowledge, the band energy of ZnO is 3.37 eV and that for anatase TiO_2 is 3.20 eV. The band energy of ZnO/TNPs composites is lower than that for ZnO and TiO_2. Therefore, the red shift of ZnO/TiO_2NTs samples could be attributed to the contribution of each of
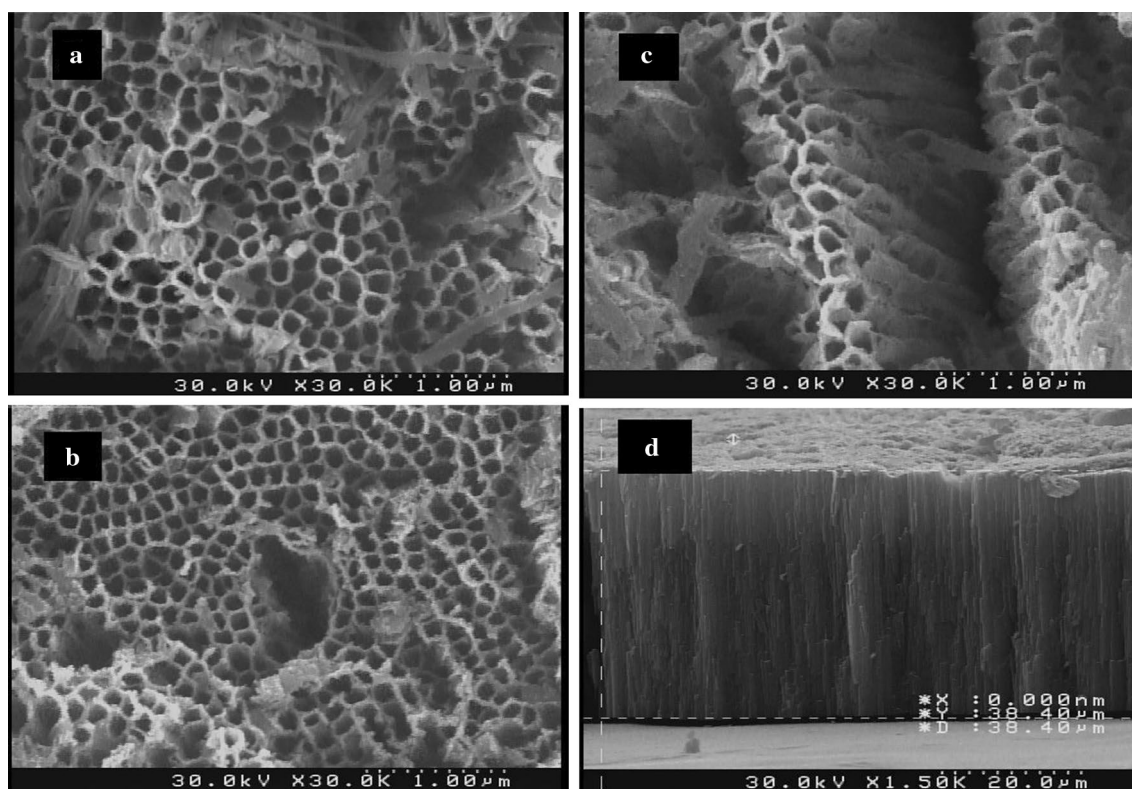
Fig. 3 **a–c** SEM top-view images of the different samples; **a** ZnO/TNPs1; **b** ZnO/TNPs2 and **c** ZnO/TNPs3. **d** Cross-sectional image of the ZnO/TNPs sample
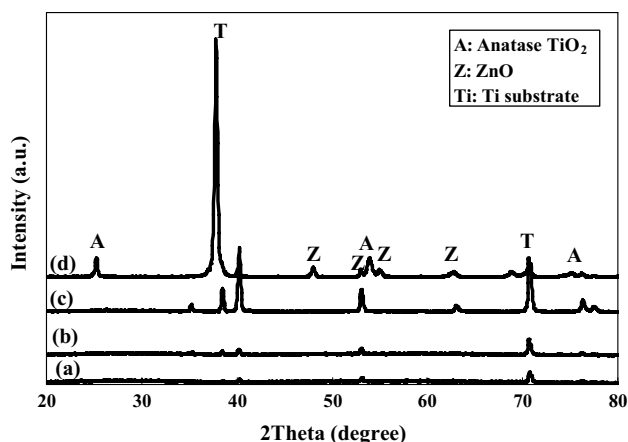
Fig. 4 XRD patterns of samples; **a** as-prepared TNPs; **b** as-prepared ZnO/TNPs1; **c** TNPs annealed at 400 °C, and **d** ZnO/TNPs1 annealed at 400 °C

the oxide component ZnO and TiO_2. Mixed crystal helps to the red shift of the absorption edge. This red shift may be owing to the high crystallinity of ZnO and significant differences in the surface state, which promote the separate efficiency of photogenerated charges and extend the range of excited spectrum, and this finding is supported by data from other study. In other words, it can be said that the presence of ZnO can modify the optical properties,

to extend the range of the excited spectrum and favor the absorption of solar energy in the visible region. It also has been found that a red shift occurs, as immersion time increased, causing an increase of the amount of zinc oxide [39].

Photocatalytic activity of different samples (TNPs and ZnO/TNPs) was followed through degradation of methylene blue as a function of irradiation time with visible light (Fig. 7a). The first, methylene blue degradation experiments were conducted under visible light irradiation to evaluate direct photolysis without the addition of any catalyst. The concentration of methylene blue remained nearly constant after 120 min of irradiation. Thus, no obvious degradation of methylene blue was observed in this time period. In addition, a dark control experiment was conducted, indicating that the adsorption of methylene blue onto the surface of the catalyst in the absence of visible light radiation was negligible. The photocatalysis results indicated that the photocatalytic process was very effective in the removal of methylene blue and it was observed that the degradation of methylene blue was enhanced using ZnO/TNPs samples. Figure 7a shows photocatalytic activity of different samples that were followed through degradation of methylene blue as a function of irradiation time with visible light. Under the irradiation of visible light, undoped TNPs sample showed almost no photocatalytic activity, but the ZnO-decorated titania nanoporous (ZnO/TNPs) samples showed photocatalytic

233,890 counts in 60 seconds
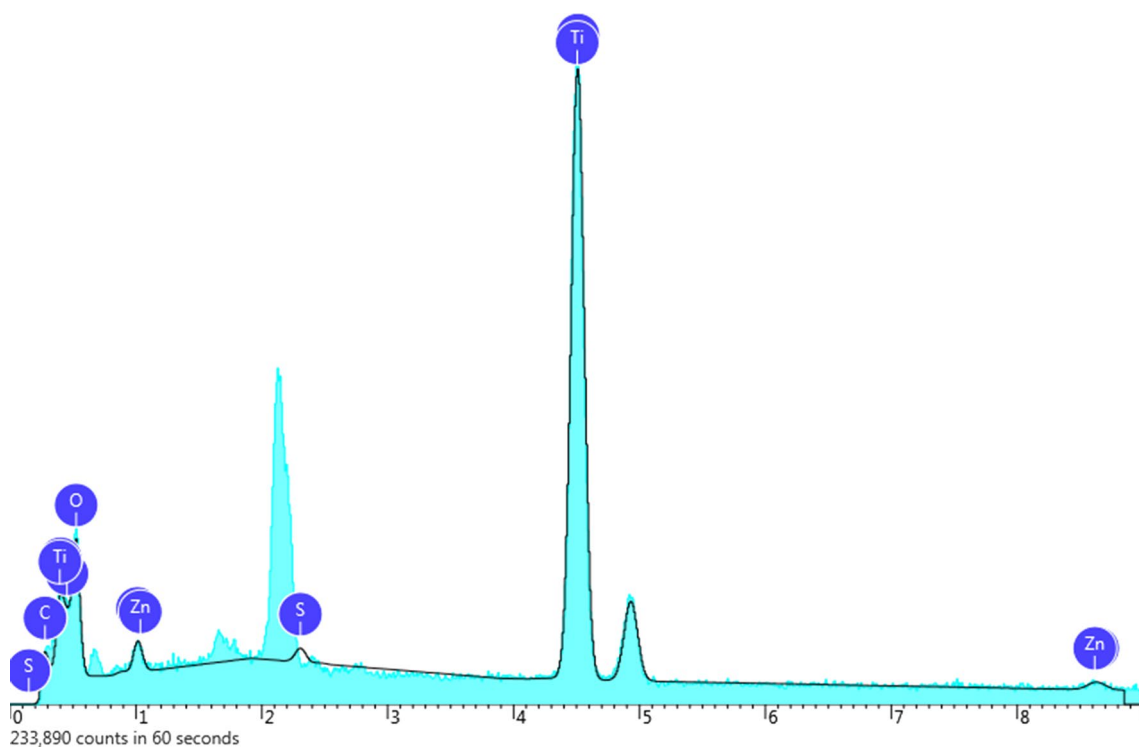
**Fig. 5** EDX spectra of ZnO/TNPs sample
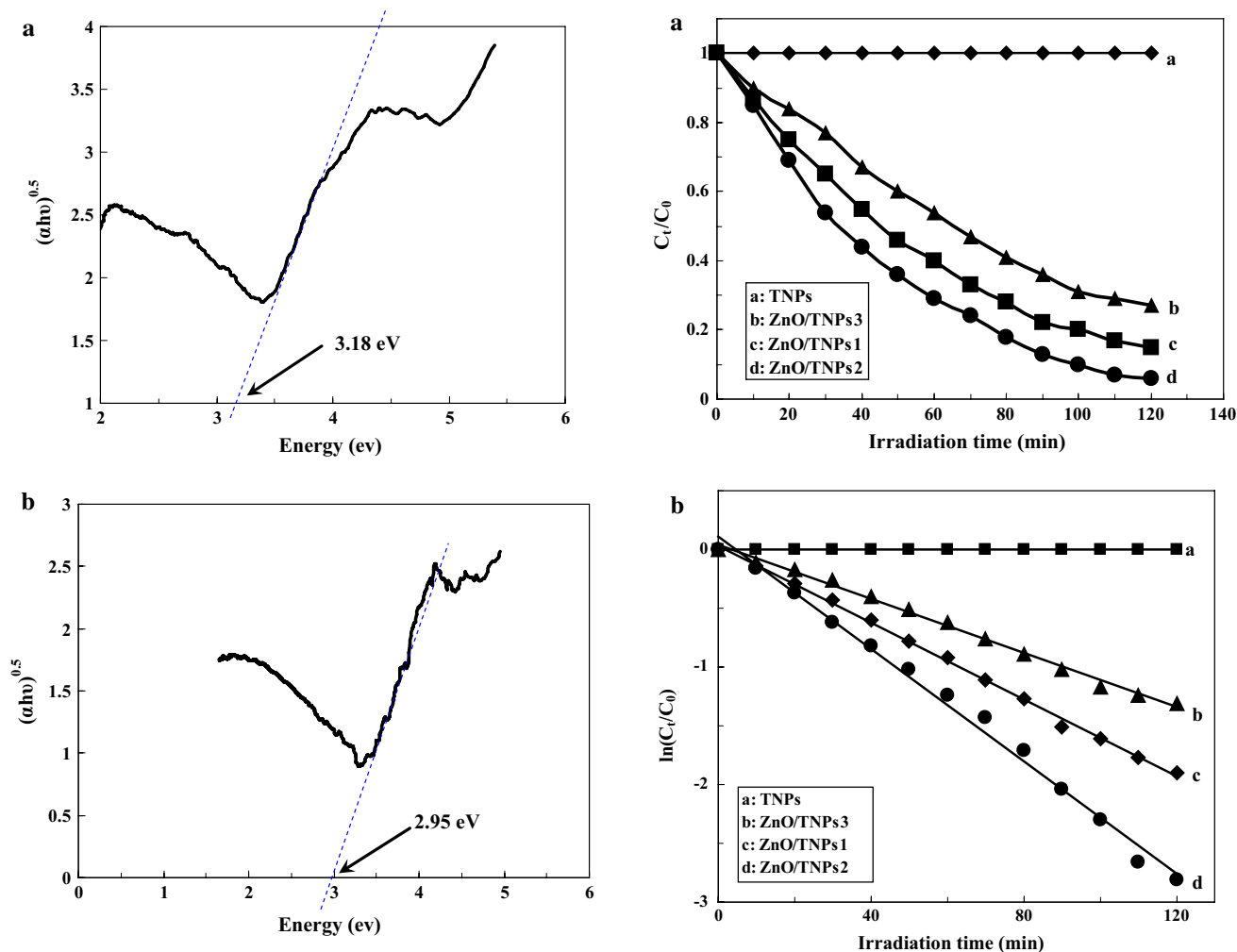
Fig. 6 Plot of $(\alpha h\upsilon)^{1/2}$ vs. $h\upsilon$ employed to calculate the band gap value of samples; **a** TNPs and **b** ZnO/TNPs2

activity. Figure 7a shows that the sample ZnO/TNPs2 exhibited better photocatalytic activity than other samples under visible light illumination.

The experimental results of the TiO$_2$ photocatalytic degradation of different organic contaminants revealed that the corresponding data fit to the Langmuir–Hinshelwood kinetic model that can be simplified to a pseudo-first-order kinetic equation as follows for diluted solutions [40–47]:

$$\ln\left(\frac{C_t}{C_0}\right) = -k_{\text{app}}\, t \qquad (2)$$

where C_t is the concentration of methylene blue at time t, C_0 is the equilibrium concentration after adsorption and k_{app} is the apparent rate constant. From the plot of $\ln(C_t/C_0)$ vs. irradiation time (Fig. 7b), we can see that the plots
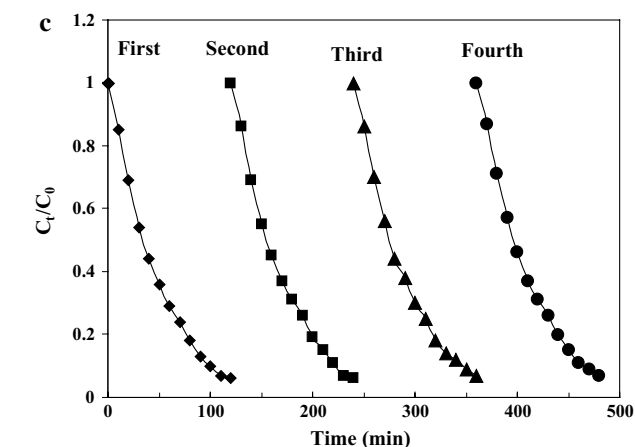
Fig. 7 **a** The photocatalytic degradation of methylene blue (MB) over the different samples under visible light irradiation. **b** Ln(C_t/C_0) vs. irradiation time plot. **c** Photocatalyst stability test of ZnO/TNPs2 for photocatalytic degradation of MB

Table 2 The apparent first-order rate constant (k) of photocatalytic degradation of methylene blue for different samples

Samples	Apparent rate constant, k (min^{-1})	Correlation coefficient, R^2
TNPs	–	–
ZnO/TNPs1	1.64×10^{-2}	0.998
ZnO/TNPs2	2.39×10^{-2}	0.993
ZnO/TNPs3	1.15×10^{-2}	0.995

represent a straight line and the slope of linear regression can be equal to the apparent first-order rate constant k. The apparent first-order rate constants and correlation coefficients corresponding to Fig. 7b are listed in Table 2.

The stability of a photocatalyst was also important to its practical application for it can be regenerated and reused. We investigated the cyclic stability of sample ZnO/TNPs2 by monitoring the catalytic activity during successive cycles of use. As shown in Fig. 7c, after a four-cycle experiment, this catalyst exhibited similar catalytic performance without significant deactivation, revealing its high stability after multiple reuses.

Conclusion

In this work, ZnO-decorated titania nanoporous (ZnO/TNPs) films have been fabricated via a feasible anodization combined by a chemical bath deposition technique. The morphology and structure were characterized by FE-SEM, XRD and EDX. SEM images illustrate that ordered nanoporous with the tubes diameter of 80–110 nm and wall thickness in the range of 30–60 nm are fabricated on the surface of titanium. Diffuse reflectance spectra show an improvement in the visible absorption relative to bare TNPs. ZnO/TNPs composites have excellent photocatalytic performance. The sample ZnO/TNPs2 exhibited better photocatalytic activity than other samples. Also this photocatalyst showed good stability and it could be recycled several times without significant loss of its activity. These inexpensive ZnO/TNPs samples prepared free of noble metals are interesting candidates to drive photochemical reactions.

References

1. Z.L. Wang, Adv. Mater. **15**, 432–436 (2003)
2. A. Kudo, Y. Miseki, Chem. Soc. Rev. **38**, 253–278 (2009)
3. M.M. Momeni, Y. Ghayeb, F. Mohammadi, J. Mater. Sci. Mater. Electron. **26**, 685–692 (2015)
4. F.X. Xiao, ACS. Appl. Mater. Interfaces **4**, 7055–7063 (2012)
5. S.Z. Chu, K. Wada, S. Inoue, S. Todoroki, Chem. Mater. **14**, 266–272 (2002)
6. Z. Miao, D. Xu, J. Ouyang, G. Guo, X. Zhao, Y.N. Tang, Nano Lett. **2**, 717–720 (2002)
7. S.J. Limmer, T.P. Chou, G.Z. Cao, J. Mater. Sci. **39**, 895–901 (2004)
8. Z.R. Tian, J.A. Voigt, J. Liu, B. Mckenzie, H. Xu, J. Am. Chem. Soc. **125**, 12384–12385 (2003)
9. P. Roy, S. Berger, P. Schmuki, Angew. Chem. Int. Ed. **50**, 2904–2939 (2011)
10. M.G. Hosseini, M.M. Momeni, M. Faraji, Electroanalysis **23**, 1654–1662 (2011)
11. M.G. Hosseini, M.M. Momeni, Appl. Catal. A **427**, 35–42 (2012)
12. H. He, P. Xiao, Y. Zhang, Y. Jia, Y. Yang, Z. Qiao, J. Alloys. Compd **522**, 63–68 (2012)
13. M.M. Momeni, M.G. Hosseini, J. Mater. Sci. Mater. Electron. **25**, 5027–5034 (2014)
14. Z. Liu, X. Zhang, S. Nishimoto, M. Jin, D.A. Tryk, T. Murakami, A. Fujishima, J. Phys. Chem. C **112**, 253–259 (2008)
15. Q. Zheng, B.X. Zhou, J. Bai, L.H. Li, Z.J. Jin, J.L. Zhang, J.H. Li, Y.B. Liu, W.M. Cai, X.Y. Zhu, Adv. Mater. **20**, 1044–1049 (2008)
16. N. Lu, X. Quan, J.Y. Li, S. Chen, H.T. Yu, G.H. Chen, J. Phys. Chem. C **111**, 11836–11842 (2007)
17. I. Paramasivam, J.M. Macak, P. Schmuki, Electrochem. Commun. **10**, 71–75 (2008)
18. T. Tatsuma, S. Saitoh, Y. Ohko, A. Fujishima, Chem. Mater. **13**, 2838–2842 (2001)
19. M.M. Momeni, Y. Ghayeb, M. Davarzadeh, J. Electroanal. Chem. **739**, 149–155 (2015)
20. R. Subasri, T. Shinohara, Electrochem. Commun. **5**, 897–902 (2003)
21. M.M. Momeni, Y. Ghayeb, J. Alloys, Compd **637**, 393–400 (2015)
22. J. Li, C.J. Lin, J.T. Li, Z.Q. Lin, Thin Solid Films **519**, 5494–5502 (2011)
23. R. Subasri, S. Deshpande, S. Seal, T. Shinohara, Solid State. Lett **9**, B1–B4 (2006)
24. M.J. Zhou, N. Zhang, L. Zhang, J.H. Yan, Mater. Corros. **64**, 996–1000 (2013)
25. M.M. Momeni, Y. Ghayeb, M. Davarzadeh, J. Mater. Sci. Mater. Electron. **26**, 1560–1567 (2015)
26. S.H. Ko, D. Lee, H.W. Kang, K.H. Nam, J.Y. Yeo, S.J. Hong, C.P. Grigoropoulos, H.J. Sung, Nano Lett. **11**, 666–671 (2011)
27. J.F. Lei, L.B. Li, X.H. Shen, K. Du, J. Ni, C.J. Liu, W.S. Li, Langmuir **29**, 13975–13981 (2013)
28. N.X. Wang, C.H. Sun, Y. Zhao, S.Y. Zhou, P. Chen, L. Jiang, J. Mater. Chem. **18**, 3909–3911 (2008)
29. F. Gu, L.L. Gai, W. Shao, C.Z. Li, L.S. Mende, Chem. Commun. **47**, 8400–8402 (2011)
30. M. Agrawal, S. Gupta, A. Pich, N.E. Zafeiropoulos, M. Stamm, Chem. Mater. **21**, 5343–5348 (2009)
31. X.D. Yan, C.W. Zou, X.D. Gao, W. Gao, J. Mater. Chem. **22**, 5629–5640 (2012)
32. Y.Z. Lei, G.H. Zhao, M.C. Liu, Z.N. Zhang, X.L. Tong, T.C. Cao, J. Phys. Chem. C **113**, 19067–19076 (2009)
33. L.E. Greene, M. Law, B.D. Yuhas, P.D. Yang, J. Phys. Chem. C **111**, 18451–18456 (2007)
34. S.I. Na, S.S. Kim, W.K. Hong, J.W. Park, J. Jo, Y.C. Nah, T. Lee, D.Y. Kim, Electrochim. Acta **53**, 2560–2566 (2008)
35. R.S. Mane, W.J. Lee, H.M. Pathan, S.H. Han, J. Phys. Chem. B **109**, 24254–24259 (2005)

36. R. Liu, W.D. Yang, L.S. Qiang, H.Y. Liu, J. Power, Sources **220**, 153–159 (2012)
37. S. Panigrahi, D. Basak, Nanoscale **3**, 2336–2341 (2011)
38. G.S. Pozan, A. Kambur, Chemosphere **105**, 152–159 (2014)
39. R. Liu, W.D. Yang, L.S. Qiang, H.Y. Liu, J. Power, Sources **220**, 153–159 (2012)
40. M.M. Momeni, M. Hakimian, A. Kazempour, Ceram. Int. **41**, 13692–13701 (2015)
41. A.K.L. Sajjad, S. Shamaila, B. Tian, F. Chen, J. Zhang, Appl. Catal. B **91**, 397–405 (2009)
42. M.M. Momeni, Appl. Surf. Sci. **357**, 160–166 (2015)
43. A.K.L. Sajjad, S. Shamaila, B. Tian, F. Chen, J. Zhang, J. Hazard. Mater. **177**, 781–791 (2010)
44. M.M. Momeni, Appl. Phys. A **119**, 1413–1422 (2015)
45. I.K. Konstantinou, T.A. Albanis, Appl. Catal. B **42**, 319–335 (2003)
46. M.M. Momeni, Y. Ghayeb, Z. Ghonchegi, Ceram. Int. **41**, 8735–8741 (2015)
47. J.M. Herrmann, Top. Catal. **34**, 49–65 (2005)